AIAA JOURNAL
Vol. 33, No. 7, July 1995

New Mode Tracking Methods in Aeroelastic Analysis

M. S. Eldred*
University of Michigan, Ann Arbor, Michigan 48109
V. B. Venkayya†
U.S. Air Force Flight Dynamics Directorate, Wright–Patterson Air Force Base, Ohio 45433
and
W. J. Anderson‡
University of Michigan, Ann Arbor, Michigan 48109

Within the context of analysis of finite element models, a methodology is developed for the tracking of complex eigenvalues and eigenvectors through changes in aeroelastic eigenvalue problems. The goal is to eliminate difficulties caused by mode switching (i.e., frequency crossing). Two new methods for mode tracking are presented and compared with an existing method. The first new method, the complex higher order eigenpair perturbation algorithm, is based on a perturbation expansion of the eigenproblem. It iteratively computes changes in the eigenpairs due to parameter perturbations with the important feature of maintaining the correspondence between the baseline and perturbed eigenpairs. The second new method is the complex cross-orthogonality check method which uses mass biorthogonality of the left and right eigenvectors to re-establish correspondence after a standard reanalysis. Applications of mode tracking technology are presented in *V–g* and *p–k* subsonic aeroelastic analyses. Each application procedure is outlined and examples are given. Recommendations are made based on method ease of use and robustness in the example problems.

Nomenclature

$[A]$ = aerodynamic matrix from the doublet lattice method; complex, nonhermitian; function of geometry, k, and M
b = reference semichord of a wing
$[C]$ = cross-orthogonality check matrix
c = weighting factor for the homogeneous solution in the eigenvector perturbation calculation
$[D]$ = coefficient matrix in the eigenvector perturbation solutions, singular
$\{F\}$ = static pseudoload vector appearing in eigenvector perturbation calculations
f = frequency, Hz
g = artificial structural damping in V–g aeroelastic analysis
k = reduced frequency, $(\omega b/V)$
$[k]$ = modal stiffness matrix, diagonal
M = Mach number
$[m]$ = modal mass matrix, diagonal
p = root of the p–k aeroelastic analysis equation, $k(\gamma + i)$
q = dynamic pressure $(\frac{1}{2}\rho V^2)$
V = air speed
$\{V\}$ = particular solution for eigenvector perturbation from Nelson's method
$[Z]$ = matrix of $\{z\}$ column vectors
$\{z\}$ = air-on vibratory mode of normal mode participation factors, eigenvector in V–g and p–k aeroelastic analysis
α = real part of c weighting factor
β = imaginary part of c weighting factor
γ = true damping in p–k aeroelastic analysis
Δ = perturbation symbol denoting exact change from a reference
θ = component phase to be rotated to 0 in phase correction enforcement
λ = complex eigenvalue
ξ = collection of terms in solution for c
ρ = air density
ω = circular frequency, rad/s

Subscripts

i = associated with the ith eigenpair
L = associated with the left eigenvector
R = associated with the right eigenvector

Superscripts

(k) = aeroelastic increment number
T = standard transpose, hermitian transpose denoted by $\overline{()}^T$
0 = baseline value
1 = perturbed value resultant from parameter change, e.g., $()^1 = ()^0 + \Delta()$

Introduction

MODE tracking is a general technology applicable to eigenvalue problems which have variable parameters. Eigenvalue problems can be classified as being either self-adjoint or nonself-adjoint. In the self-adjoint case, energy is conserved within the system model, the eigenpairs are real, and the left eigenvectors are identical to the right eigenvectors. The structural eigenvalue problem is an example of this, and mode tracking is applied to structural optimization in Ref. 1. In the nonself-adjoint case, energy is not conserved within the system model, the eigenvalues and eigenvectors are complex in general, and the left eigenvectors differ from the right eigenvectors. Aeroelastic eigenvalue problems are examples of nonself-adjointness, with the nonconservatism resulting from the fluid flow. It is worth emphasizing that structural optimization and aeroelastic analysis are not the only members of the self-adjoint and nonself-adjoint classes to which mode tracking techniques can be applied. Rather, this technology is applicable whenever modal data needs to be uniquely identified throughout a sequence of variations in the parameters of the eigenproblem statement (see Ref. 2).

In subsonic aeroelastic analysis, the air-on vibratory frequencies and modes are ordered by their air-off frequencies (free vibration frequencies). As the airspeed is changed, the vibratory frequencies will change and mode crossings can occur. Mode crossings that

Received April 5, 1994; revision received Jan. 10, 1995; accepted for publication Jan. 10, 1995. This paper is declared a work of the U.S. Government and is not subject to copyright protection in the United States.

*Graduate Research Assistant, Department of Aerospace Engineering, currently Senior Member of Technical Staff, Structural Dynamics Department, Sandia National Laboratories, Albuquerque, NM 87185. Member AIAA.

†Principal Scientist. Associate Fellow AIAA.

‡Professor of Aerospace Engineering. Senior Member AIAA.

are not properly tracked can cause misidentification of aeroelastic phenomena, since the observed variations of aeroelastic modes with respect to the incremental parameter will be erroneous. When this occurs, the factors leading to flutter and divergence are not properly understood and attempts to improve performance will be misguided and likely unsuccessful.

Mode tracking techniques are used to establish correspondence among the sets of point solutions that are generated at the discrete parameter values of the incremental aeroelastic analysis. To generate curves for specific vibratory modes, it is necessary to determine the modal identity of each point solution. Several methods for the connection of these point solutions currently exist. First, point solutions may be connected by hand using the judgement of the analyst. This can quickly become a daunting and confusing task. Second, modes can be correlated based on complex eigenvalue similarity. This is the simplest automated approach and the least robust. A more sophisticated approach proposed by Desmarais and Bennett[3] for V–g analysis relies on the shape of the characteristic polynomial and uses Laguerre iteration to converge from a previous to a corresponding current eigenvalue. In this method, the increments in reduced frequency that are taken must be very small, and correlation failure occurs when the closest zero of the polynomial to the starting point is not the correct corresponding eigenvalue. Lastly, a recent method proposed by van Zyl[4] improves on the Desmarais and Bennett method by correlating the modes based on complex inner products between current and previous right eigenvectors. This latter method bears similarities to the complex cross-orthogonality check (C-CORC) method presented herein, but neglects the very useful mass biorthogonality property of the left and right complex eigenvectors (see C-CORC method discussion).

The two new methods presented herein, the complex higher order eigenpair perturbation algorithm (C-HOEP) and C-CORC, perform automated mode tracking based on robust mathematical arguments, specifically through perturbation expansion or through mass biorthogonality.

Mode Tracking Methods for Nonself-Adjoint Eigenvalue Problems

Mode tracking algorithms maintain correspondence between baseline and perturbed eigenpairs (set of frequencies and modes on adjacent iterations or increments). They either replace or augment the eigenproblem reanalysis phase of an optimization algorithm (see Ref. 1) or incremental process (such as aeroelastic analysis). In aeroelastic analysis, this entails tracking the complex eigenpairs as either reduced frequency (V–g method, p–k method) or airspeed (p–k method) is incremented.

Two new methods are proposed for use in mode tracking for nonself-adjoint problems: the complex higher order eigenpair perturbation algorithm and the complex cross-orthogonality check method.

Complex Higher Order Eigenpair Perturbations (C-HOEP)

This method is an extension of Ref. 5 in that it performs a perturbation expansion on a nonself-adjoint eigenproblem for which the associated eigenpairs are complex. All perturbation terms are retained, leading to coupled equations for the eigenvalue perturbation and the left and right eigenvector perturbations. The approach is general and will be illustrated by way of specific examples: perturbation of the reduced frequency in the V–g aeroelastic analysis equation and perturbation of the reduced frequency or the velocity in the p–k aeroelastic analysis equation.

Aeroelastic Analysis, V–g Equation

The eigenproblem statement for V–g aeroelastic analysis can be written as follows:

$$[(1+ig)[k]-\omega^2([m]+[A])]\{z_R\}=\{0\} \tag{1}$$

where $[A]$ is the complex, nonhermitian aerodynamic matrix derived from the doublet lattice method,[6,7] g is the artificial structural damping necessary to sustain harmonic oscillation (which is required for the unsteady aerodynamics), ω is the frequency of the harmonic oscillation, $[k]$ and $[m]$ are diagonal modal stiffness and mass, respectively, and $\{z_R\}$ is the right eigenvector made up of complex normal mode participation factors. This equation can be rewritten

$$[[k]-\lambda([m]+[A])]\{z_R\}=\{0\} \tag{2}$$

where

$$\lambda=\omega^2/(1+ig) \tag{3}$$

is the complex eigenvalue. The associated left eigenproblem is

$$\overline{\{z_L\}}^T[[k]-\lambda([m]+[A])]=\{0\}^T \tag{4}$$

Perturbing the reduced frequency k in Eq. (2) affects the aerodynamic matrix and the eigenpairs, giving the following equation written for the ith eigenpair:

$$[[k]-(\lambda_i^0+\Delta\lambda_i)([m]+[A^0]+[\Delta A])]\left(\left\{z_R^0\right\}_i+\{\Delta z_R\}_i\right)=\{\mathbf{0}\} \tag{5}$$

After canceling the baseline solution, the full-order eigenvalue perturbation equation is derivable by premultiplying by either the left or the right baseline eigenvector. In the former case, the baseline solution can be canceled a second time, giving

$$\Delta\lambda_i=\frac{-\lambda_i^0\overline{\left\{z_L^0\right\}_i}^T[\Delta A]\left\{z_R^1\right\}_i}{\overline{\left\{z_L^0\right\}_i}^T([m]+[A^1])\left\{z_R^1\right\}_i} \tag{6}$$

In the latter case, the baseline solution cannot be canceled again, and the following equation results:

$$\Delta\lambda_i=\frac{\overline{\left\{z_R^0\right\}_i}^T([k]-\lambda_i^0([m]+[A^1]))\{\Delta z_R\}_i-\lambda_i^0\overline{\left\{z_R^0\right\}_i}^T-[\Delta A]\left\{z_R^0\right\}_i}{\overline{\left\{z_R^0\right\}_i}^T([m]+[A^1])\left\{z_R^1\right\}_i} \tag{7}$$

If left eigenvector data are available, Eq. (6) is preferable to Eq. (7) due to its convergence characteristics.

The corresponding eigenvector perturbation equations are

$$[D^1]_i\{\Delta z_R\}_i=\{F_R\}_i \tag{8}$$

$$\overline{\{\Delta z_L\}_i}^T[D^1]_i=\overline{\{F_L\}_i}^T \tag{9}$$

where

$$[D^1]_i\equiv[k]-\lambda_i^1([m]+[A^1]) \tag{10}$$

is singular and

$$\{F_R\}_i\equiv\left(\lambda_i^0[\Delta A]+\Delta\lambda_i([m]+[A^1])\right)\left\{z_R^0\right\}_i \tag{11}$$

$$\overline{\{F_L\}_i}^T\equiv\overline{\left\{z_L^0\right\}_i}^T\left(\lambda_i^0[\Delta A]+\Delta\lambda_i([m]+[A^1])\right) \tag{12}$$

are static pseudoloads. Equations (8) and (9) are solvable since they are "consistent" ($\{F_R\}_i$ is orthogonal to $\{z_L^1\}_i$ and $\{F_L\}_i$ is orthogonal to $\{z_R^1\}_i$). This biorthogonality of the pseudoload vectors is true for nonself-adjoint problems in general.

The total solution for $\{\Delta z_R\}_i$ is made up of homogeneous and particular solutions. Since $[D^1]_i\{z_R^1\}_i=\{\mathbf{0}\}$, $\{z_R^1\}_i$ is a homogeneous solution for $\{\Delta z_R\}_i$ in Eq. (8). The total solution for $\{\Delta z_R\}_i$ is then a sum of the particular solution $\{V_R\}_i$ and a weighted $\{z_R^1\}_i$:

$$\{\Delta z_R\}_i=c_{R_i}\left\{z_R^1\right\}_i+\{V_R\}_i \tag{13}$$

Equation (13) must be altered since $\{z_R^1\}_i$ is unknown. Expanding $\{z_R^1\}_i$ and collecting $\{\Delta z_R\}_i$ terms gives

$$\{\Delta z_R\}_i=\frac{c_{R_i}}{1-c_{R_i}}\left\{z_R^0\right\}_i+\frac{1}{1-c_{R_i}}\{V_R\}_i \tag{14}$$

Employing conditions of magnitude normalization for the current and projected systems

$$\overline{\{z_R^0\}_i}^T \{z_R^0\}_i = \overline{\{z_R^1\}_i}^T \{z_R^1\}_i = 1 \tag{15}$$

and substituting Eq. (14) for $\{\Delta z_R\}_i$ in an expansion of Eq. (15) yields the following equation for c_{R_i}:

$$c_{R_i}\overline{c_{R_i}} - c_{R_i} - \overline{c_{R_i}} = \xi_{R_i} \tag{16}$$

where

$$\xi_{R_i} = \overline{\{z_R^0\}_i}^T \{V_R\}_i + \overline{\{V_R\}_i}^T \{z_R^0\}_i + \overline{\{V_R\}_i}^T \{V_R\}_i \tag{17}$$

is a real number. Equation (16) involves two unknowns, because the weighting factor c_{R_i} is complex in general. Thus, the magnitude normalization of Eq. (15) is not enough to define a unique complex eigenvector, and an additional condition must be imposed. This additional condition is a phase correction, which forces the maximum magnitude component of a complex eigenvector to have zero phase by multiplying the vector by a unit magnitude scalar of opposite phase. This correction is unique despite the phase discontinuity at $\pm\pi$, and can be viewed as a complex extension of the sign convention defined for real eigenvectors (see iteration invariance discussion in Ref. 1). That is, real eigenvectors require a normalization and sign convention in order to be defined uniquely, and complex eigenvectors require a normalization and phase correction in order to be defined uniquely.

Two approaches can be taken in enforcing the phase correction condition. The first approach is to assume that c_{R_i} is real. The desired root is then

$$c_{R_i} = 1 - \sqrt{1 + \xi_{R_i}} \tag{18}$$

In this case, the homogeneous solution contribution in Eq. (13) is not rotated in phase, and the phase-correction condition is not enforced on each C-HOEP iteration. Instead, the phase of the perturbed eigenvectors must be corrected after C-HOEP convergence. This approach is simpler but less rigorous.

The more rigorous approach is to enforce the phase correction condition on each C-HOEP iteration. That is, use c_{R_i} to rotate the homogeneous solution in Eq. (13) such that the phase of the perturbed eigenvector satisfies the phase-correction condition. This approach is preferred. First, it must be recognized from Eq. (14) that

$$\{z_R^1\}_i = \{z_R^0\}_i + \{\Delta z_R\}_i = 1/(1 - c_{R_i})\left(\{z_R^0\}_i + \{V_R\}_i\right) \tag{19}$$

Therefore, to enforce zero phase on a component of $\{z_R^1\}_i$, the phase of $1/(1-c_{R_i})$ must cancel the phase of the corresponding component of $\{z_R^0\}_i + \{V_R\}_i$. Denoting the phase of the corresponding component of $\{z_R^0\}_i + \{V_R\}_i$ by θ_R and letting

$$c_{R_i} = \alpha_R + i\beta_R \tag{20}$$

where the vector index is not to be confused with the imaginary number i, it is straightforward to show that

$$\beta_R = (\alpha_R - 1)\tan\theta_R \tag{21}$$

Substituting Eq. (21) into Eq. (20) and substituting the result into Eq. (16), one finds the solution for α_R,

$$\alpha_R = 1 - \sqrt{1 - \frac{\tan^2\theta_R - \xi_{R_i}}{\tan^2\theta_R + 1}} \tag{22}$$

where the extraneous root has been deleted. Equations (17) and (20–22) define a c_{R_i} value which yields unique, normalized, and phase-corrected perturbed eigenvectors. Also, Eqs. (20–22) reduce to Eq. (18) for $\theta_R = 0$.

The magnitude normalization and phase-correction conditions for the left eigenvectors are the same as for the right eigenvectors. Denoting the phase of the corrected component of $\{z_L^0\}_i + \{V_L\}_i$ by θ_L, the following equations are solved in order for the left eigenvector perturbation:

$$\xi_{L_i} = \overline{\{z_L^0\}_i}^T \{V_L\}_i + \overline{\{V_L\}_i}^T \{z_L^0\}_i + \overline{\{V_L\}_i}^T \{V_L\}_i \tag{23}$$

$$\alpha_L = 1 - \sqrt{1 - \frac{\tan^2\theta_L - \xi_{L_i}}{\tan^2\theta_L + 1}} \tag{24}$$

$$\beta_L = (\alpha_L - 1)\tan\theta_L \tag{25}$$

$$c_{L_i} = \alpha_L + i\beta_L \tag{26}$$

$$\{\Delta z_L\}_i = \frac{c_{L_i}}{1 - c_{L_i}}\{z_L^0\}_i + \frac{1}{1 - c_{L_i}}\{V_L\}_i \tag{27}$$

The left eigenvectors will be required if Eq. (6) is to be used in an incremental process. The same modified and decomposed $[D^1]_i$ matrix may be used in the computation of particular solutions for $\{\Delta z_L\}_i$ and $\{\Delta z_R\}_i$ so long as the same pivotal element is used for the left and right systems (this is the standard procedure; consult Ref. 8 for details of Nelson's method).

Relaxation has proved to be useful in accelerating the convergence of the eigenpair perturbation technique. When repetitive overprediction of the eigenpair perturbations occurs (resulting from very large parameter perturbations or convergence criteria that are not strict enough over a series of increments), underrelaxation of $\Delta\lambda_i$, $\{V_R\}_i$, or $\{V_L\}_i$ estimates can be performed to tame the oscillations. These oscillations have been observed to be phase oscillations, which are detected if the current change in an estimate and the change on the previous C-HOEP iteration differ in phase by more than $\pi/2$. In the example problem of the Applications section, only $\Delta\lambda$ estimates are underrelaxed, and a constant underrelaxation factor of 0.6 is used.

The algorithm flowchart for C-HOEP is shown in Fig. 1. Iteration 0 consists of obtaining an initial estimate of the eigenvalue perturbations from a first-order approximation to Eq. (6) or (7). The nonlinear iterations are then performed, which consist of solution of the approximately singular eigenvector perturbation equations [Eqs. (8) and (9)], followed by the full-order update for the eigenvalue perturbation [Eq. (6) or (7)]. Solution for the eigenvector perturbations requires the computation of the particular solutions of Eqs. (8) and (9) ($\{V_R\}_i$ and $\{V_L\}_i$) by Nelson's method,[8] calculation of c_{R_i} from Eqs. (17) and (20–22), and c_{L_i} from Eqs. (23–26), and

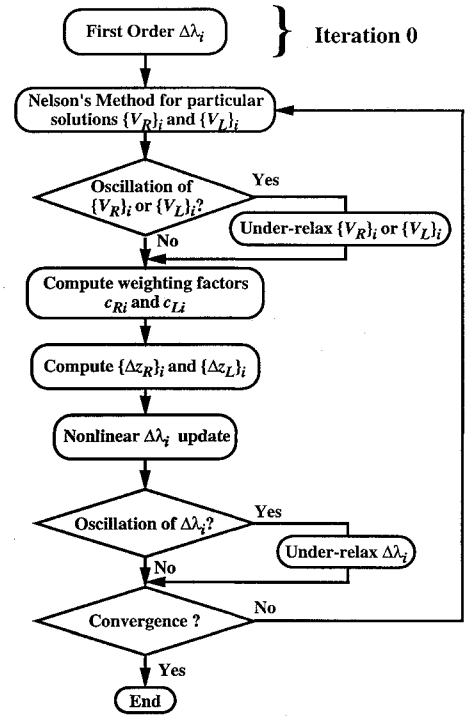

Fig. 1 C-HOEP algorithm with underrelaxation.

finally solution of Eqs. (14) and (27) for $\{\Delta z_R\}_i$ and $\{\Delta z_L\}_i$. Underrelaxation of $\Delta\lambda_i$, $\{V_R\}_i$, or $\{V_L\}_i$ estimates is performed when oscillation is detected. These iterations continue until the convergence criterion is satisfied. Mode tracking is possible because the computations involve the ith eigenpair only, creating a direct correspondence between current and projected data.

Aeroelastic Analysis, p–k Equation

The p–k aeroelastic analysis problem, as presented by Hassig.[9] Equation is based on incremental solution of the following equation:

$$\left[[k] - \tfrac{1}{2}\rho V^2[A] + (V/b)^2 p^2[m]\right]\{z_R\} = \{\mathbf{0}\} \tag{28}$$

where

$$p = k(\gamma + i) \tag{29}$$

and $[A]$ differs from that of the V–g method by the factor $2k^2/\rho b^2$. Implementations of the p–k method by MSC/NASTRAN and ASTROS[10,11] place a p/k term on the out-of-phase portion of the aerodynamics (imaginary part of $[A]$). This modification better predicts near zero frequency behavior,[12] specifically static instability in short period modes (full airplane instability of zero frequency and positive damping), and divergence (cantilever wing instability of zero frequency and zero damping), but it complicates the perturbation equations and will not be presented here. For simplicity in the perturbation equations, the eigenvalue will be defined as

$$\lambda = (V/b)^2 p^2 = \omega^2(\gamma + i)^2 \tag{30}$$

where the proper ω, γ pair are defined for a λ value by the fact that $\omega \geq 0$. The dynamic pressure will be absorbed into $[A]$ which will be denoted as $[qA]$. Then, $[\Delta qA]$ will account for changes in air speed as well as changes in reduced frequency. The right eigenproblem can now be written

$$[[k] - [qA] + \lambda[m]]\{z_R\} = \{\mathbf{0}\} \tag{31}$$

and the associated left eigenproblem is

$$\overline{\{z_L\}}^T [[k] - [qA] + \lambda[m]] = \{\mathbf{0}\}^T \tag{32}$$

The perturbation equations for expansion of Eqs. (31) and (32) for the ith eigenpair are

$$\Delta\lambda_i = \frac{\overline{\{z_L^0\}}_i^T [\Delta qA]\{z_R^1\}_i}{\overline{\{z_L^0\}}_i^T [m]\{z_R^1\}_i} \tag{33}$$

and

$$[D^1]_i\{\Delta z_R\}_i = \{F_R\}_i \tag{34}$$

$$\overline{\{\Delta z_L\}}_i^T [D^1]_i = \overline{\{F_L\}}_i^T \tag{35}$$

where

$$[D^1]_i \equiv [k] - [qA^1] + \lambda^1[m] \tag{36}$$

and

$$\{F_R\}_i \equiv ([\Delta qA] - \Delta\lambda_i[m])\{z_R^0\}_i \tag{37}$$

$$\overline{\{F_L\}}_i^T \equiv \overline{\{z_L^0\}}_i^T ([\Delta qA] - \Delta\lambda_i[m]) \tag{38}$$

Equations (14), (17), (20–22), and (23–27) also apply to p–k aeroelastic analysis and $\Delta\lambda_i$, $\{\Delta z_R\}_i$, and $\{\Delta z_L\}_i$ are computed in the same manner as described in the V–g aeroelastic analysis section.

Complex Cross-Orthogonality Check (C-CORC)

The C-CORC method is a complex extension of the method of Gibson.[13] For nonself-adjoint eigenvalue problems, one can make use of the biorthogonality property of the left and right eigenvectors to recorrelate the complex modes. The expression for the $[C]$ matrix is dependent on the mass operator in the eigenproblem statement. For V–g aeroelastic analysis, the $[C]$ matrix is

$$[C] = \overline{\left[Z_L^{(k-1)}\right]}^T ([m^{(k)}] + [A^{(k)}])\left[Z_R^{(k)}\right] \tag{39}$$

where k and $k-1$ are the current and previous increments, respectively. In p–k aeroelastic analysis, the expression is similar:

$$[C] = \overline{\left[Z_L^{(k-1)}\right]}^T [m^{(k)}]\left[Z_R^{(k)}\right] \tag{40}$$

If the $[C]$ matrix is diagonally dominant in magnitude, then no mode switching has occurred; if the matrix is not diagonally dominant, the locations of the dominant values can be used to recorrelate the current iteration modes. Obviously, these calculations require left eigenvector information which is not generally computed. Also, using the proper conjugation of the left eigenvectors is essential to success of the method. To measure the assurance with which the correlations are made, corruption indices (the second largest magnitude in a column of $[C]$ divided by the first largest magnitude, i.e., the runner-up correlation divided by the selected correlation; see Ref. 1) are calculated.

A variant on this approach was proposed by van Zyl,[4] in which a correlation index is defined as

$$C_{ij} = \frac{\left|\overline{\left\{z_R^{(k-1)}\right\}}_i^T \left\{z_R^{(k)}\right\}_j\right|}{\left|\left\{z_R^{(k-1)}\right\}_i\right|\left|\left\{z_R^{(k)}\right\}_j\right|} \tag{41}$$

Since right eigenvectors are neither self- nor mass orthogonal for nonself-adjoint eigenvalue problems, use of the biorthogonality property in C-CORC allows for more range in the correlation indices and, therefore, easier distinction of proper correlations than van Zyl's approach. That is, the correlation indices in an orthogonality-based method will tend toward zero for the noncorrelated modes and toward unity for the correlated modes, whereas the correlation indices for van Zyl's method may all tend toward unity, making corruption indices greater and the distinction of the proper correlation more difficult.

Applications

It is important to distinguish between the different solution techniques used in aeroelastic optimization and incremental aeroelastic analysis. An excellent report by O'Connell et al.[14] discusses the various computational procedures for aeroelastic problems. In aeroelastic optimization, points of zero damping are sought directly, typically by repeated solution of the flutter determinant.[15,16] These points of instability can be ordered by air speed or by frequency and may switch order under a design change. This would be an interesting area to apply mode tracking technology in the future.

In incremental aeroelastic analysis, the case of interest in this paper, air-on vibratory modes are computed at various increments of a parameter. This parameter is the reduced frequency (k) in V–g type aeroelastic analysis and is the air speed (V) in p–k type aeroelastic analysis. These incremental analysis methods show the variation of damping as a function of the incremental parameter and aid in the identification of flutter phenomena (such as hump modes, e.g., the near instability of mode 4 in Fig. 4 near 900 m/s) that might otherwise be missed.

V–g Aeroelastic Analysis

In V–g aeroelastic analysis, the analysis steps through reduced frequency (k) values, extracting complex eigenpairs on each step, until the desired flutter points are obtained (when the artificial damping required for harmonic oscillation is greater than that available from the structure). Mode tracking is used to automatically connect these point solutions, so that the effect of the parameter variations on the aeroelastic vibratory modes can be studied. Existing methods for mode tracking in V–g aeroelastic analysis include manual

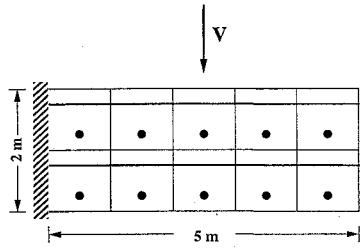

Fig. 2 Rectangular wing with doublet lattice discretization.

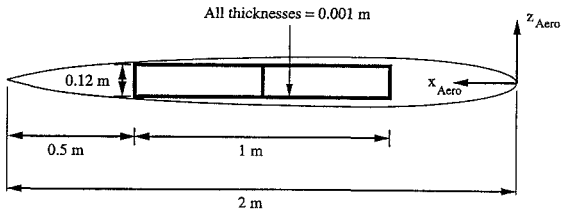

Fig. 3 Wing box cross section.

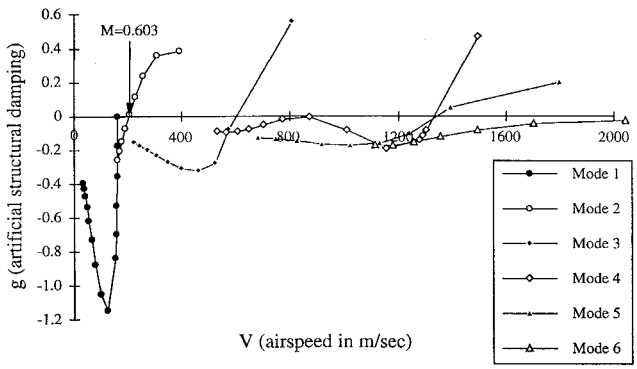

Fig. 4 V–g plot for $0 \leq k \leq 1$.

correlation, correlation based on complex eigenvalue similarity, the method of Desmarais and Bennett,[3] and the method of van Zyl,[4] as discussed in the Introduction.

The new approaches to be demonstrated are C-HOEP and C-CORC. As the reduced frequency k is incremented, new aerodynamic matrices are computed or interpolated from known values. In C-HOEP, the change in the aerodynamic matrix $[\Delta A]$ drives the perturbations to the eigenvalues and right and left eigenvectors, and one iteration loop to convergence is performed for each incremental k value. In C-CORC, a reanalysis based on the new $[A]$ and a recorrelation based on $[C]$ are performed for each incremental k value. Both methods are demonstrated in the following example and compared with the method of van Zyl.

Example 1: Mode Tracking in V–g *Aeroelastic Analysis for a Rectangular Wing*

The aerodynamic planform and doublet lattice discretization for the rectangular wing are shown in Fig. 2. The underlying structure was kept simple and is an aluminum cantilever beam with a two bay box cross section (Fig. 3). The structural box is centered in the wing chord for simplicity, which has a destabilizing effect since it causes the structural center of mass to be well aft of the aerodynamic center. A total of six normal modes is retained, three each of bending and torsion. For sea level density ($\rho = 1.225$ kg/m^3), matched point divergence occurs for $V = 165$ m/s ($M = 0.485$) and matched point flutter occurs for $V = 205$ m/s ($M = 0.603$). For Mach 0.603 at sea level, a V–g analysis for k varying from 1.0 to 0.0 was performed, resulting in Figs. 4 and 5. In these figures, only the analysis points with zero damping accurately represent the dynamics (since g is an artifice) and only the analysis points at $V = 205$ m/s represent matched points (since the analysis is run for sea level density and $M = 0.603$). Also, the velocity values computed for the higher modes are far from subsonic for this range of k values. These are the weaknesses of the V–g analysis method. The most

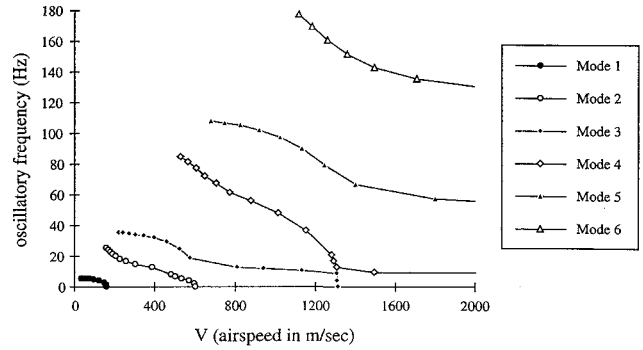

Fig. 5 V–f plot for $0 \leq k \leq 1$.

important thing to note is apparent in Fig. 5, where the modes are seen to veer away from one another. That is, frequency crossings are not a problem for this example, and simply ordering the modes by frequency magnitude is sufficient.

Whereas frequency crossings may be rare for a clean wing, with modes that are strongly coupled by the aerodynamics, this is not true for more complex configurations, where some modes are not greatly affected by the aerodynamic changes.

Performance of the mode tracking methods was evaluated for this example problem. The methods were programmed in MATLAB[17] and used to "connect the dots" in Figs. 4 and 5. The lack of frequency crossings allows evaluation of the mode tracking methods well past their region of convergence, since the proper correlations are known with assurance. Detailed data and results are documented in Ref. 2.

In C-HOEP, use of left eigenvector data is desirable, and only a relatively small penalty is paid for calculating the left eigenvector perturbations in addition to the right eigenvector perturbations since the same modified and decomposed $[D^1]_i$ matrix is used for the left and right calculations. In fact, it is often cheaper to calculate both the left and right eigenvector perturbations using left and right eigenvector data than to calculate right eigenvector perturbations using right eigenvector data only. This is due to the faster convergence and fewer number of C-HOEP iterations required. Thus, calculation of both eigenvector perturbations is recommended for C-HOEP in incremental processes.

As expected, increasing the perturbation size decreases the performance of both methods, and proper correlation of the modes is less assured. Decreasing assurance of modal correlation is manifested in higher numbers of iterations required for convergence in C-HOEP and in higher corruption indices in C-CORC.

C-HOEP tends to be slightly more computationally expensive than C-CORC, although the number of modes tracked and the convergence tolerance used in C-HOEP, and the extraction routine used and the range of modes extracted prior to C-CORC are all variables which cloud the efficiency issue. Relative efficiency of the mode tracking methods, however, is not as important for aeroelastic analysis as it is in structural optimization,[1] since the matrices are typically of low order (modal coordinates) and both C-HOEP and C-CORC computational expenses are dwarfed by the expense of calculating the aerodynamic matrices.

There are large changes in the vibratory modes near $k = 0.4$, causing the methods to have convergence problems. When nearing flutter, the vibratory mode shapes become very similar, as if a classical frequency coalescence were occurring. Mode tracking with the C-HOEP, C-CORC, and van Zyl methods is tested in true incremental fashion for the range $0.1 \leq k \leq 0.4$ in order to test robustness in this difficult region. The initial k is 0.5 and uniform decrements are taken of 0.1 with the baseline updated at each step. Performance of the methods is measured in the number of failed correlations (fc) that are made, in the number of iterations needed to reach convergence for C-HOEP, and in the maximum corruption for C-CORC and van Zyl. A failed correlation occurs in C-HOEP if the algorithm converges to an incorrect eigenpair due to excessively large perturbations in the eigenproblem. A failed correlation occurs in C-CORC and van Zyl if the mode shapes become too similar and the largest magnitude component in a column of the $[C]$ matrix corresponds to an incorrect mode. Since there is a priori knowledge

Table 1 Robustness of C-HOEP, C-CORC, and van Zyl's method near flutter points

	C-HOEP		C-CORC		van Zyl	
k	iters	fc	MCorr*	fc	MCorr*	fc
0.40	5	0	0.212	0	0.980	0
0.30	6	0	0.337	0	0.989	0
0.20	8	0	0.432	0	0.994	0
0.10	20	0	1.437	1	1.004	1

Table 2 Robustness of mode tracking methods near flutter points

	C-HOEP		C-CORC		van Zyl	
k	iters	fc	MCorr*	fc	MCorr*	fc
0.45	3	0	0.109	0	0.972	0
0.40	4	0	0.107	0	0.978	0
0.35	4	0	0.136	0	0.983	0
0.30	4	0	0.185	0	0.988	0
0.25	5	0	0.192	0	0.991	0
0.20	5	0	0.267	0	0.993	0
0.15	9	0	0.681	0	1.010	1
0.10	10	0	0.632	0	——	——
0.05	15	0	0.990	0	——	——

of the proper correlations, a modified maximum corruption index (MCorr*) is calculated for measuring C-CORC and van Zyl performance. This corruption index divides the largest noncorrelated value in a column of $[C]$ by the properly correlated value. A value of greater than 1.0 shows correlation failure; whereas in standard practice, where the correct correlations are not known a priori, values of greater than 1.0 are not possible. Table 1 shows the results.

It can be seen from the failed correlation count that C-HOEP is the most robust for the difficult region of k values. Similar mode shapes near flutter can cause C-CORC and van Zyl to fail, whereas C-HOEP can still track modes despite this mode shape similarity. Note that it takes more iterations to converge in the C-HOEP method as $k = 0.0$ is approached since the change in air speed is increasing. Also, as evidenced by its very high corruption values, van Zyl's method has little range in the correlation values, making it difficult to distinguish the proper correlations. This lack of differentiation is due to the fact that van Zyl's correlation indices do not make use of the eigenvector biorthogonality property.

An additional test case was performed in which the initial k is again 0.5, and increments of 0.05 are taken until the final k value of 0.05 is attained. A similar result occurs, as shown in Table 2, in that C-CORC nearly fails at the final increment ($k = 0.05$) with a maximum corruption of 0.99 and for which C-HOEP converges in 15 iterations with no failed correlations. For this range of k, van Zyl's method is noticeably less robust, in that it fails at $k = 0.15$.

Once a mode tracking method fails in an incremental process, it is difficult to recover since the following iteration modes are being correlated with or computed from a bad set. The only known way to recover is to detect the failure, back up, and decrease the step size.

p–k Aeroelastic Analysis

The p–k aeroelastic analysis is performed differently from the V–g analysis since V is the incremental parameter instead of k. Since k is an unknown, an iterative loop must be performed to match the $[A]$ matrix to the p root. That is, a value for k must be assumed to calculate an $[A]$ matrix, which gives a p root in the eigenpair computation, which yields a new k estimate from Eq. (29). This new k defines a new $[A]$, and iteration is performed until agreement is achieved. Convergence on a value of k in this manner has been observed to be unstable near flutter points, even with use of under- and overrelaxation of k. In particular, underrelaxation sometimes cannot take large oscillations in the predicted k value (hunting) when flutter points are being approached. For a commercial installation, a more robust method for converging on k will be required.

It is very important to recognize the increase in logical complexity that this indefiniteness in k causes. Unlike the V–g method in which a given k value defines exactly n vibratory modes for a modalized equation of order n, the p–k method has the feature that there may be more than n modes at a given airspeed for which the aerodynamics match the p root. There are still only n vibratory modes for a given value of k, but since k and, therefore, $[A]$ are variable, each converged vibratory mode is now a product of its own distinct eigenvalue problem, and the number of eigenpairs is no longer rigidly defined. In a sense, the eigenvalue problem is not well posed since the stiffness operator depends on the eigenvalue. These additional modes are extraneous roots of the p–k aeroelastic equation and are typically explained to be aerodynamic poles (roots derived from the unsteady aerodynamics alone which are not associated with the structure). The extraneous roots can cause problems for the mode tracking algorithms, since the algorithms can mistakenly lock onto one of these roots if the extraneous root is similar to the correct root.

Implementation of a mode tracking method for p–k aeroelastic analysis is, then, a two step process. Whereas, in V–g aeroelastic analysis, one C-HOEP convergence loop or C-CORC recorrelation is performed for each incremental k value for each mode, an extra iteration loop must be performed in p–k aeroelastic analysis to converge on a k value for each V value for each mode. Since, at most, one mode is meaningful for a given k value, C-HOEP has the advantage that it can track that one mode of interest and not be concerned with the other modes.

The calculation of the aerodynamic matrices is a major part of the computational expense. For this reason, a goal of a p–k aeroelastic analysis algorithm is to minimize the number of evaluations of $[A]$ while maintaining the ability to generate matched points (analysis points for which the density, velocity, and Mach number reflect a standard atmosphere condition). One approach is to interpolate $[A]$ in terms of k for several prescribed values of Mach number, and then attempt to match a meaningful density and Mach number to each velocity. This approach is taken by the implementations of the p–k method in MSC/NASTRAN and ASTROS. In another approach, the density (along with speed of sound and altitude) is fixed, and an incremental change in velocity is accompanied by a proportional change in Mach number. The aerodynamic matrix must then be interpolated for both k and M (preferably with a surface spline). The assumption is that fixing the altitude and varying the Mach number is more physically meaningful than fixing Mach numbers and varying altitude. This latter approach is employed in the following p–k example problem, so each analysis point in the figures represents a matched point condition for a constant altitude.

Example 1: Mode Tracking in p–k *Aeroelastic Analysis for a Rectangular Wing*

The same rectangular wing planform and structure (Figs. 2 and 3) are used. Again, six normal modes are retained, three each of bending and torsion. For sea level density and matching Mach number, vibratory modes are extracted for eight subsonic velocities in the range 100 m/s $\leq V \leq$ 300 m/s. Unlike the V–g analysis results, frequency crossings are present for the p–k analysis. Without mode tracking, the frequency crossings are not tracked and the resulting V–γ and V–f plots for the first three modes are as shown in Figs. 6 and 7 (where failed correlations are shown with dashed lines). With mode tracking, the frequency crossings are properly tracked and the

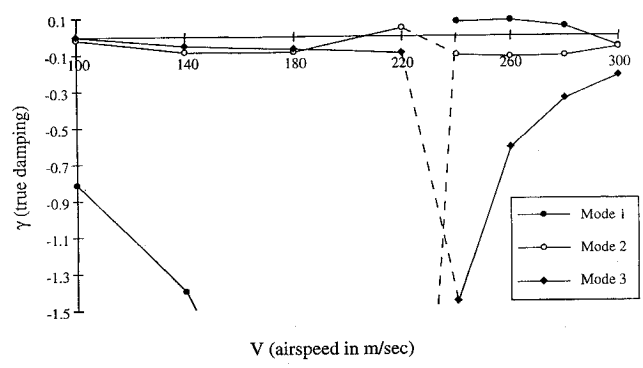

Fig. 6 V–γ plot with no mode tracking.

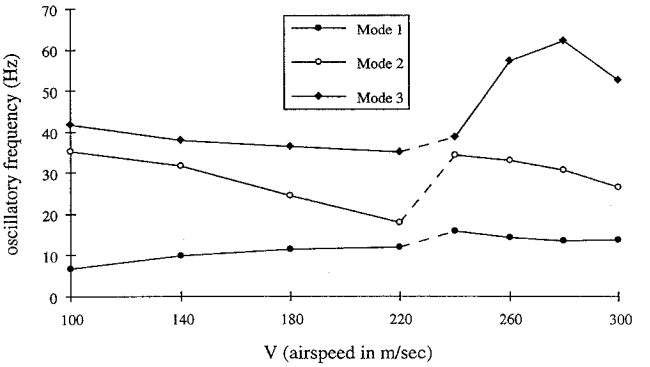

Fig. 7 *V–f* plot with no mode tracking.

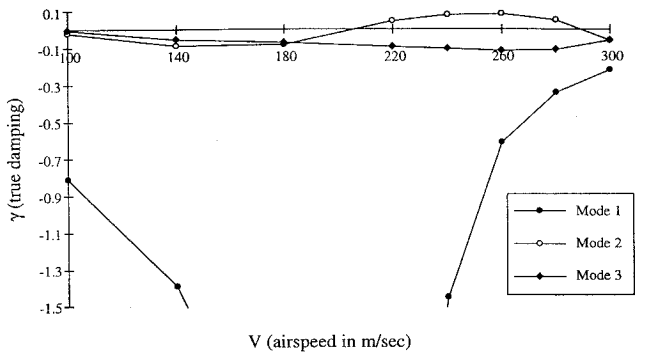

Fig. 8 *V–γ* plot with mode tracking.

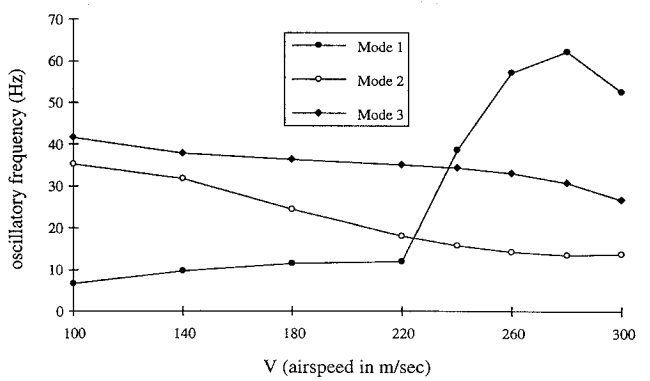

Fig. 9 *V–f* plot with mode tracking.

correct $V-\gamma$ and $V-f$ plots are as shown in Figs. 8 and 9. Mode tracking is especially important in $p-k$ aeroelastic analysis because, in addition to the converged vibratory modes (such as those shown in Figs. 6–9), the nonconverged modes (when matching p to $[A]$ for a mode, there are $n-1$ other nonconverged modes) and the extraneous modes (aerodynamic poles) can also cross frequencies with the modes of interest. Thus, in $p-k$ analysis, there are many more modes available to create confusion than in $V-g$ analysis.

Comparing the flutter results of the $V-g$ and $p-k$ aeroelastic analysis methods (Figs. 4 and 8), it is evident that mode 2 flutters at an airspeed of 205 m/s for both analysis methods. Comparing the divergence results of the $V-g$ and $p-k$ aeroelastic analysis methods, it can be seen that the $p-k$ method fails in predicting divergence. Whereas mode 1 in Fig. 8 resembles the divergence mode of Fig. 4, it never achieves the zero frequency/zero damping condition characteristic of divergence modes. Presumably, placing the p/k term on the out-of-phase portion of the aerodynamics in the $p-k$ aeroelastic equation formulation (as discussed earlier) would remedy this shortcoming.

Performance of the C-HOEP, C-CORC, and van Zyl mode tracking methods in $p-k$ aeroelastic analysis has been evaluated for the first three aeroelastic vibratory modes (Tables 3–5). There is less difference between C-CORC and van Zyl's method for $p-k$ analysis than for $V-g$ analysis, since the mass operator used in C-CORC for $p-k$ analysis is simply the diagonal modal mass matrix (the identity matrix for mass normalized normal modes). Therefore, the comparison between C-CORC and van Zyl illustrates the difference between correlation based on previous left and previous right eigenvectors, without the added difference of the presence of a complex, nonhermitian mass operator in C-CORC.

Table 3 Comparison of incremental mode tracking methods for mode 1

	C-HOEP		C-CORC		van Zyl	
V	MIter	fc	MCorr	fc	MCorr	fc
100	5	No	0.15	No	0.19	No
140	14	No	0.51	No	0.70	No
180	13	No	0.48	No	0.91	No
220	8	No	0.15	No	0.75	No
260	13	No	0.43	No	0.80	No
300	19	Yes	0.84	Yes	0.79	Yes

Table 4 Comparison of incremental mode tracking methods for mode 2

	C-HOEP		C-CORC		van Zyl	
V	MIter	fc	MCorr	fc	MCorr	fc
100	8	No	0.73	No	0.32	No
140	15	No	0.52	No	0.87	No
180	18	No	0.41	No	0.60	No
220	10	No	0.33	No	0.49	No
260	6	No	0.19	No	0.48	No
300	6	No	0.20	No	0.40	No

Table 5 Comparison of incremental mode tracking methods for mode 3

	C-HOEP		C-CORC		van Zyl	
V	MIter	fc	MCorr	fc	MCorr	fc
220	10	No	0.34	No	0.39	No
240	12	No	0.27	No	0.38	No
260	20	No	0.50	No	0.51	No
280	25	Yes	0.83	Yes	0.98	No
300	22	Yes	0.11	Yes	0.86	Yes

In tracking mode 1 (Table 3), the data were extracted for increment of 40 m/s from a starting point of 100 m/s with an initial k guess of 1.0. The MIter heading denotes the maximum number of C-HOEP iterations required to converge within a $10^{-6}\%$ tolerance on λ_i^1 over all iterations on k for the given air speed. Likewise, the MCorr heading denotes the maximum corruption value in the C-CORC and van Zyl methods for the mode being tracked over all iterations on k for the given airspeed. The fc headings tell whether or not a failed correlation occurred for the mode tracking method. C-HOEP and C-CORC both show moderate difficulty for the 140, 180, and 260 m/s increments, through high numbers of maximum iterations in C-HOEP and high maximum corruption values in C-CORC. It is more difficult to distinguish relative correlation assurance in van Zyl's method, since the corruption indices have less range than those of C-CORC. At the 300-m/s increment, for example, the larger number of iterations required in C-HOEP, 19, and the larger corruption value in C-CORC, 0.84, provide clues to the failure of these methods, whereas the corruption value of 0.79 in van Zyl's method does not stand out from the values for previous velocity increments. All three methods fail for the 300-m/s increment. The velocity increments must be decreased in order to verify the proper correlation for $V =$ 300 m/s, and when this is done, the mode tracking methods are successful in tracking mode 1 into a region of large oscillations in k that underrelaxation cannot tame. Here, a more robust method for converging on k is needed. In these decreased increment analyses for mode 1, no clear performance advantage was found among the three mode tracking methods since the locations and types of correlation failures coincided exactly.

For vibratory mode 2, Table 4 shows the performance data for increments of 40 m/s from an initial velocity of 100 m/s (initial k guess = 1.0). For this mode, all three methods succeed in mode tracking for each increment, with the most difficulty shown on the third increment for C-HOEP, on the first increment for C-CORC,

and on the second increment for van Zyl's method. This shows that the three methods are very different, in that one method can have difficulty with an increment for which another method exhibits high correlation assurance.

For vibratory mode 3, Table 5 shows the performance data for increments of 20 m/s from an initial velocity of 220 m/s (initial k guess = 1.2). Both C-HOEP and C-CORC fail on the final two velocity increments, and van Zyl's method nearly fails at 280 m/s before failing at 300 m/s. The exact nature of the failures differ. On the $V = 280$ m/s increment, C-HOEP fails by converging to an extraneous root (aerodynamic pole), and C-CORC fails by erroneously correlating mode 2 instead of mode 3. C-CORC remains locked onto mode 2 for the final increment with a low corruption index of 0.11. This low value might mislead an analyst into high correlation assurance if the failure on the previous increment was not detected. On the final increment, van Zyl's method fails by converging to the same aerodynamic pole which caused C-HOEP to fail. Decreasing the velocity increments to 10 m/s allows the mode tracking methods to progress further (no table). C-HOEP fails on the $V = 290$ m/s increment by again converging to an aerodynamic pole, whereas C-CORC survives near failure at the $V = 290$ m/s increment (with a maximum corruption of 0.92) and fails on the final increment by again correlating mode 2 instead of mode 3. Van Zyl's method succeeds for each increment, surviving a high corruption of 0.94 on the final increment. Refining the velocity increments to 5 m/s steps (no table) allows C-CORC to successfully mode track through each increment, with a maximum corruption value of 0.71 on the $V = 300$ m/s increment. C-HOEP, on the other hand, fails on the final increment ($V = 300$ m/s) by once again converging to an aerodynamic pole. Van Zyl's method succeeds again, with the corruption on the final increment decreasing slightly to 0.90.

Van Zyl's method appears to be more robust for p–k aeroelastic analysis, since it is more successful in tracking mode 3 for the velocity increments shown. Also, it appears that C-CORC and van Zyl's method are more robust than C-HOEP in their ability to avoid aerodynamic poles. More research is needed on these extraneous roots and how they can be avoided. All three methods are successful in tracking vibratory modes through changes in reduced frequency and through increments in air speed, provided that the velocity increment is decreased sufficiently. This is the only way to verify the correct correlations.

Conclusions

New mode tracking techniques, C-HOEP and C-CORC, have been developed and applied to the automated connection of point solutions in subsonic aeroelastic analysis. They have been compared to an existing technique proposed by van Zyl. All three methods are successful to varying degrees in mode tracking for V–g and p–k aeroelastic analyses. By eliminating problems caused by mode switching, the factors leading to flutter and divergence will be better understood and attempts to improve performance will be more effective.

Compared with the computation and interpolation of the $[A]$ matrices for various values of k and M, the mode tracking methods are very inexpensive. Therefore, ease of use and robustness of the methods are the key issues when it comes to selecting a mode tracking technique.

In V–g aeroelastic analysis, C-HOEP has been shown to be more robust in the example problem than C-CORC, and both C-HOEP and C-CORC easily outperform van Zyl's method. Although similar to C-CORC, van Zyl's method lacks the use of the biorthogonality property, making it more difficult to distinguish the proper correlations due to a reduced range in the correlation indices. Near flutter points, different flutter modes can become very similar, causing vector product correlation methods (C-CORC and van Zyl) to fail. C-HOEP can successfully track modes near flutter despite mode shape similarity.

The performance trend for V–g analysis completely reverses itself for p–k analysis, although the performance differences are of less magnitude. In p–k analysis, van Zyl's method outperforms C-CORC and C-HOEP despite its lack of range in correlation indices. This result is somewhat surprising in that C-HOEP and C-CORC have stronger mathematical bases. It is believed that the simple mass operator used in p–k analysis (the diagonal modal mass matrix, which is the identity matrix for mass normalized normal modes) is the reason for the success of van Zyl's approach, in that van Zyl's approach does not suffer in this case from not accounting for a mass operator. C-HOEP performs well but is slightly less effective than the other two, since it has been susceptible to converging on extraneous roots of the p–k aeroelastic equation (aerodynamic poles). More research is needed on these extraneous roots in order to better understand how they can be avoided.

General recommendations for the choice of a mode tracking method can be made. For the specific application of p–k aeroelastic analysis, van Zyl's method works well due to the simplicity of the p–k mass operator and is recommended, at least until it is learned how the extraneous roots can be avoided with C-HOEP. However, for V–g aeroelastic analysis and other nonself-adjoint eigenvalue problems with general mass operators, van Zyl's method is not recommended. For these problems, C-CORC may be preferable due to its simplicity and ease of integration. Or, if the problem is more difficult and large mode changes are possible, then C-HOEP is recommended due to its robustness.

Acknowledgments

The authors appreciate discussions with Max Blair of the Air Force Flight Dynamics Laboratory on details of the doublet lattice method, with Ronald Taylor of the University of Dayton Research Institute on mode tracking needs in aeroelastic analysis, and with Erwin Johnson of the MacNeal–Schwendler Corp. on details of the p–k aeroelastic analysis method. The authors also wish to acknowledge the helpful comments and suggestions made at the 34th Structures, Structural Dynamics, and Materials Conference.

References

[1]Eldred, M. S., Venkayya, V. B., and Anderson, W. J., "Mode Tracking Issue in Structural Optimization," *AIAA Journal* (to be published).

[2]Eldred, M. S., "Full Order Eigenpair Perturbations with Mode Tracking Applications in Aeroelasticity and Optimization," Ph.D. Dissertation, Univ. of Michigan, Ann Arbor, MI, 1993.

[3]Desmarais, R. N., and Bennett, R. M., "An Automated Procedure for Computing Flutter Eigenvalues," *Journal of Aircraft*, Vol. 11, No. 2, 1974, pp. 75–80.

[4]van Zyl, L. H., "Use of Eigenvectors in the Solution of the Flutter Equation," *Journal of Aircraft*, Vol. 30, No. 4, 1993, pp. 553, 554.

[5]Eldred, M. S., Lerner, P. B., and Anderson, W. J., "Higher Order Eigenpair Perturbations," *AIAA Journal*, Vol. 30, No. 7, 1992, pp. 1870–1876.

[6]Albano, E., and Rodden, W. P., "A Doublet-Lattice Method for Calculating Lift Distributions on Oscillating Surfaces in Subsonic Flows," *AIAA Journal*, Vol. 7, No. 2, 1969, pp. 279–285.

[7]Blair, M., "A Compilation of the Mathematics Leading to the Doublet Lattice Method," WL-TR-92-3028, 1992.

[8]Nelson, R. B., "Simplified Calculation of Eigenvector Derivatives," *AIAA Journal*, Vol. 14, No. 9, 1976, pp. 1201–1205.

[9]Hassig, H. J., "An Approximate True Damping Solution of the Flutter Equation by Determinant Iteration," *Journal of Aircraft*, Vol. 8, No. 11, 1971, pp. 885–889.

[10]Rodden, W. P. (ed.), "MSC/NASTRAN Handbook for Aeroelastic Analysis, Volume I, MSC/NASTRAN Version 65," MacNeal–Schwendler Corp., 1987, p. 2.6-4.

[11]Johnson, E. H., and Venkayya, V. B., "Automated STRuctural Optimization System (ASTROS), Volume I, Theoretical Manual," Air Force Wright Aeronautical Lab., AFWAL-TR-88-3028, Wright-Patterson AFB, OH, 1988, p. 127.

[12]Hassig, H. J., "The p–k Method Revisited," Aerospace Flutter and Dynamics Council Meeting, May 1993.

[13]Gibson, W., "ASTROS-ID: Software for System Identification using Mathematical Programming," WL-TR-92-3100, 1992.

[14]O'Connell, R. F., Hassig, H. J., and Radovcich, N.A., "Study of Flutter Related Computational Procedures for Minimum Weight Structural Sizing of Advanced Aircraft," NASA CR-2607, March 1976.

[15]Bhatia, K. G., "An Automated Method for Determining the Flutter Velocity and the Matched Point," *Journal of Aircraft*, Vol. 11, No. 1, 1974, pp. 21–27.

[16]Stroud, W. J., Dexter, C. B., and Stein, M., "Automated Preliminary Design of Simplified Wing Structures to Satisfy Strength and Flutter Requirements," NASA TN D-6534, 1971.

[17]Moler, C., Herskovitz, S., Little, J., and Bangert, S., "MATLAB for Macintosh Computers: User's Guide," MathWorks, Inc., 1988.